EXAFS spectroscopic analysis of the Verwey transition in Fe_3O_4.

Gloria Subías, Joaquín García,* and Javier Blasco
Instituto de Ciencia de Materiales de Aragón, Departamento de Física de la Materia Condensada, CSIC—Universidad de Zaragoza, Pedro Cerbuna 12, 50009 Zaragoza, Spain
(Received 15 October 2004; revised manuscript received 29 November 2004; published 5 April 2005)

We present an extended x-ray absorption fine structure study at the Fe *K* edge of the local structural changes in Fe_3O_4 across the Verwey transition at $T_V \sim 120$ K. The local structure of the FeO_6 octahedra is distorted below T_V and remains unaltered during the transition, the local distortions being already present in the pseudocubic phase above T_V. The phonon modes responsible for the lattice distortion are those associated with displacements of the octahedral Fe-Fe chains. We propose that the metal-insulator transition is then caused by a change in the regime of the local distortions from a static regime at low temperatures to a dynamical one at high temperatures, the lattice dynamics above T_V being the origin for the electrical conductivity.

DOI: 10.1103/PhysRevB.71.155103 PACS number(s): 71.30.+h, 61.10.Ht, 71.38.−k, 75.50.Gg

I. INTRODUCTION

Metal-insulator transitions (MIT) are one of the most characteristic features of the electronic conduction in transition-metal oxide systems.[1] The large variety of proposed mechanisms leading to MIT makes difficult to fully establish an adequate theoretical framework to describe them properly.[2] The Verwey transition in magnetite (Fe_3O_4) at about $T_V \sim 120$ K is one of the classical examples of a first-order MIT in transition-metal oxides.[3–6] Fe_3O_4 is thought to be a half metal above T_V showing a record Curie temperature (T_C) of 860 K. At T_V, the conductivity decreases abruptly by two orders of magnitude. This MIT is related to a lattice distortion of the high-temperature phase that is cubic (inverse spinel structure, Fd-3m s. g.). The low-temperature phase is thought to be monoclinic (Cc s. g.), but it is noteworthy that it has not been fully resolved yet.[7–9] Verwey[10] described this transition as an order-disorder electronic transition based on the cation distribution on the octahedral sites of the inverse spinel structure. The formal chemical formula is $Fe_A^{+3}[Fe^{+3},Fe^{+2}]_B O_4^{-2}$, where *A* and *B* refer to the tetrahedral and octahedral sites, respectively. The disordered state above T_V is metallic due to the motion of the "extra" 3*d* electrons, hopping between the octahedral sites. Below T_V, these extra electrons become localized and a long-range charge ordering (CO) sets on the *B* sites in alternate (001) planes.

A large amount of experimental and theoretical works has been devoted to the study of this electronic CO transition since the Verwey's model was reported but no consensus has been reached so far. Several models were proposed to explain the "metallic" behavior above T_V, namely, a collective electron-band model[11–13] and a narrow polaron-band model.[3,5] For example, Cullen and Callen[11] proposed a simple band model where interatomic Coulomb repulsion is the only relevant interaction among electrons. This model predicts multiple-ordering states at the Verwey transition depending on the ratio between interatomic Coulomb repulsion and bandwidth. Recently, the issue of CO has been explored using band structure LDA+U calculations in both cubic[12] and monoclinic[13] phases. They show the opening of an energy gap at the Fermi level, explaining the MIT. However, the fact that if the charge disproportionations found in the insulating phase are of an electronic origin (CO) or determined by the structural distortions, is still disputed. On the other hand, Mott,[3] adopting Verwey's concept, suggested that magnetite can be better described as a Wigner glass above T_V, where each electron (polaron or bipolaron) is in an Anderson-localized state. Nearest-neighbor polaron hopping is then proposed as most likely mechanism for conduction. At $T=T_V$, the Wigner glass transforms discontinuously into a Wigner crystal. Despite this great number of models, there is not a CO pattern[8,10,14] able to explain the measured physical properties.[15] Furthermore, NMR[16,17] and x-ray resonant scattering experiments[18,19] disagree with the presence of CO for $T<T_V$. Moreover, recent electrical resistivity measurements on magnetite under high pressure[20] show that the Verwey transition is intrinsically a MIT and the ground state is metallic at ~8 GPa, discarding a polaronic conduction.

These results force us to reconsider the mechanism of conductivity in Fe_3O_4. The main clear fact at the Verwey transition is the existence of a structural phase transition. The crystal structure changes from cubic to at least monoclinic with decreasing temperature. The unit cell is doubled along the *c* direction due to small displacements of the atoms at T_V.[7,8] This structural change is also accompanied by a sharp discontinuity in several physical properties as the electrical resistivity, heat capacity, elastic constants or magnetization.[15] It is also quite interesting that magnetite seems to maintain locally this low-temperature structure even at temperatures above T_V. Neutron[21] and x-ray[22] diffuse scattering experiments together with the entropy change at the transition[23] are consistent with the existence of short-range correlations of the low-temperature phase above T_V. Approaching the problem of the Verwey MIT from the structural point of view, we could suppose that the loss of symmetry in the unit cell (doubling of the *c* axis) is the responsible for opening an electronic gap. In other words, the cubic symmetry above T_V permits a crossing of the bands and a finite density of states at the Fermi level whereas below T_V, the broken symmetry opens a gap. Accordingly, a band electronic model, as occurs in a generalized Peierls transition, would be an adequate model. Photoemission[24,25] and optical spectroscopy[26] studies

are in agreement with the opening of a 140 meV gap below T_V. However, they also report indications that short-range correlations exist just above T_V in the metallic phase.

Several theoretical approaches have been made to interpret these results. The model of molecular polarons by Yamada[27] is based on the electron-phonon coupling as Mott's model, but describes the Verwey transition as a cooperative ordering of molecular polarons. They are composed of two extra electrons and a local displacement mode of oxygens within the fcc primitive cell. Seo *et al.*[28] also disagree with an electronic CO model but propose that the Verwey transition arises from a bond dimerization of the Fe_B ions without charge separation.

In order to shed light on this phase transition, we present a spectroscopic study of the Verwey transition in Fe_3O_4 by using the extended x-ray absorption fine structure (EXAFS) technique at the Fe *K* edge. EXAFS technique is ideally suited for determination of the dynamic local structure around a specific absorbing atom due to the short interaction time ($\sim 10^{-15}$ s) of the photoabsorption process. EXAFS spectra were measured up to 16 $Å^{-1}$ in the wave vector *k* range with high signal-to-noise ratio in order to obtain reliable structural data. Data from Fe_3O_4 and $MnFe_2O_4$ samples were compared to ensure that the results for magnetite are statistically significant. However, EXAFS analysis of Fe_3O_4 remains complicated due to the presence of two nonequivalent (octahedral and tetrahedral) Fe sites in the crystal structure. These two oxygen shells of neighbors must be taken into account separately in order to make a reliable analysis of the data. We found that the local structure around the Fe atoms in magnetite is nearly the same above and below the Verwey transition. This result indicates that the distortion of the low-temperature monoclinic phase is already present in the high-temperature cubic phase, suggesting that the electrical conductivity above T_V should be mediated by electron-phonon coupled states.

II. EXPERIMENTAL

Polycrystalline samples of Fe_3O_4 and $MnFe_2O_4$ were obtained from crushing a piece of the respective single-crystal grown by floating zone method.[18] The samples were characterized by x-ray diffraction and magnetization measurements ensuring the right oxygen stoichiometry. Both samples are single phase at room temperature with lattice parameters of 8.396 Å for Fe_3O_4 and 8.499 Å for $MnFe_2O_4$, respectively.

X-ray absorption experiments were performed at the beam line BM29[29] of the European synchrotron radiation facility (ESRF, Grenoble, France). The storage ring operates at electron beam energy of 6 GeV with a maximum stored current of about 200 mA. A fixed-exit Si(111) double-crystal monochromator was used, the estimated resolution being $\Delta E/E \approx 8 \times 10^{-5}$ at Fe *K* edge. Harmonic rejection was achieved by 50% detuning of the two crystals from the parallel alignment. Absorption spectra ($60\ \mathrm{K} \leqslant T \leqslant 250\ \mathrm{K}$) were recorded in the transmission mode using ionization chambers as detectors. Pellets were prepared by dilution with cellulose and the amount of material was calculated to optimize the expected signal-to-noise ratio. A Fe metal foil was simultaneously measured for energy calibration.

XANES spectra were normalized to the high part of the spectrum (around 100 eV above the absorption edge) after a linear background subtraction.[30] EXAFS spectra $[\chi(k)]$ were obtained by removing the smooth atomic absorption coefficient (μ_0) by means of a cubic spline fit. The structural analysis was performed in the *R* space fitting mode using the FEFF 8.10 package.[31] Theoretical amplitudes and phases were calculated from the crystallographic data of Fe_3O_4 and $MnFe_2O_4$. The model used to fit the Fe *K* edge data includes single scattering paths up to 4 Å, i.e., the first Fe-O and the second Fe—Fe(Mn) coordination shells. It is noteworthy that a multisite-multishell analysis was performed in Fe_3O_4, due to the presence of non-equivalent iron *A* and *B* sites. Two distributions for the first oxygen coordination shell (Fe_B-O and Fe_A-O) and three distributions for the second iron coordination shell (Fe_B-Fe_B, Fe_B-Fe_A and Fe_A-Fe_A) were then considered.

III. RESULTS

Figure 1 shows the EXAFS spectra and the modulus of the Fourier transform for Fe_3O_4 and $MnFe_2O_4$ at the Fe *K*-edge at $T = 60$ K. The EXAFS spectra extend up to 16 $Å^{-1}$ with high signal-to-noise ratio. The Fourier transform (FT) of the *k*-weighted EXAFS spectra was calculated between 3.0 and 16.0 $Å^{-1}$ using a Gaussian window and structural features are noticeable up to 6 Å. We mainly observe two features. One peak at about 1.4 Å, corresponding to the first oxygen coordination shell and two further peaks between 2 and 3.5 Å mainly related to the nearest Fe_B and Fe_A/Mn_A neighbors, respectively. The comparison between Fe_3O_4 and $MnFe_2O_4$ shows that the first Fe-O peak is less intense and more asymmetric for the former compound. Similar trend is observed for the second peak. The main difference between both samples concerns to the Fe site distribution. $MnFe_2O_4$ is a normal spinel and Fe atoms mainly occupy the octahedral sites whereas Fe_3O_4 is an inverse spinel and Fe atoms occupy both, octahedral and tetrahedral sites. Therefore, the differences observed in the EXAFS spectra and their respective FT are related to the interference effect between the two contributions of the tetrahedral- and octahedral-site environments around the Fe atoms in Fe_3O_4 that it is absent in $MnFe_2O_4$.

EXAFS spectra of Fe_3O_4 and $MnFe_2O_4$ were measured at fixed temperatures from 60 K up to 250 K. The spectra at temperatures above 60 K were also collected in a wide energy range up to 1 keV ($\sim 16\ Å^{-1}$) with similar spectral signal-to-noise. This high data quality is required to determine tiny changes in the structural parameters across the phase transition. The temperature evolution of the *k*-weighted FT spectra of $MnFe_2O_4$ and Fe_3O_4 is reported in Figs. 2(a) and 2(b), respectively. Both samples show a conventional behavior for the second shell peaks, the peak height decreases as the temperature increases. On the other hand, the intensity of the first oxygen shell peak is almost constant for Fe_3O_4 and it slightly decreases for $MnFe_2O_4$. It is noteworthy that a small discontinuity in the evolution of the second peak (Fe_B-Fe_B bond distances) is observed in Fe_3O_4 at the Verwey transition, as it is displayed in detail in the inset of Fig. 2(b).

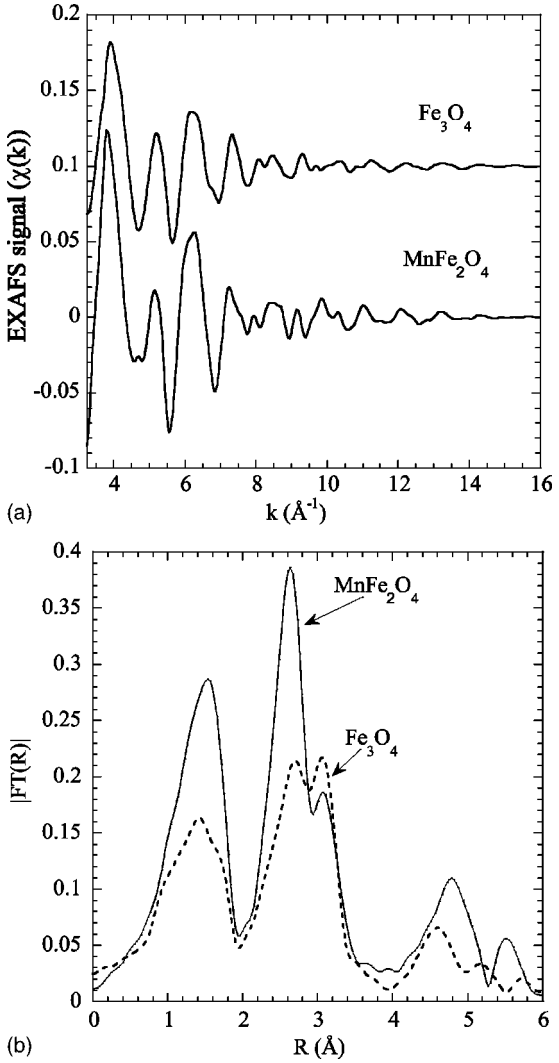

FIG. 1. (Upper panel) EXAFS ($\chi(k)$) spectra at the Fe K edge for Fe_3O_4 and $MnFe_2O_4$ samples measured at $T=60$ K. (Lower panel) Fourier transform modulus (FT) of the experimental $k\chi(k)$ signal for these samples, without phase-shift corrections.

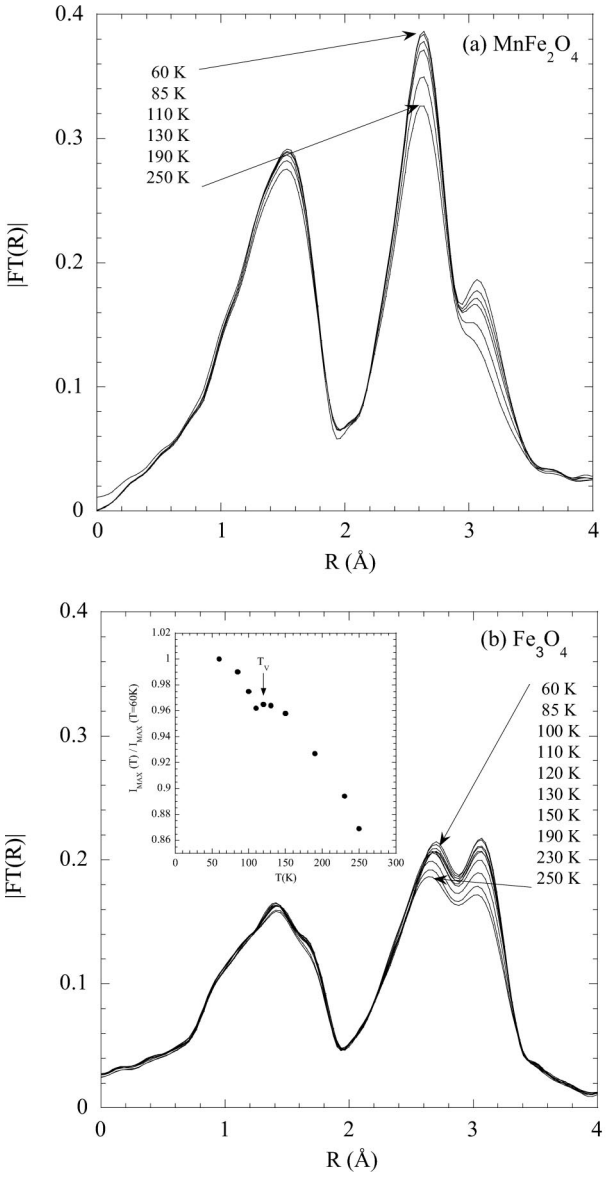

FIG. 2. (a) Fourier transform modulus (FT) of the k-weighted EXAFS spectra of $MnFe_2O_4$ at the Fe K edge as a function of temperature ($60\ \text{K} \leqslant T \leqslant 250$ K). (b) Fourier transform modulus of the k-weighted EXAFS spectra of Fe_3O_4 at the Fe K-edge as a function of temperature ($60\ \text{K} \leqslant T \leqslant 250$ K). Inset: Temperature evolution of the maximum intensity of the Fe_B-Fe_B peak normalized to the value at $T=60$ K for Fe_3O_4.

The main results of the quantitative structural analysis for the first and second coordination shells are summarized in Tables I and II, respectively. The overall reduction factor S_0^2 was fixed to the value obtained for $MnFe_2O_4$ at low temperature in such a way that the variables in the fit were the energy E_0, the interatomic distances and their Debye-Waller (DW) factors. For each sample, fits at different temperatures were also performed with a fixed value of E_0 obtained from the fit at the lowest temperature, to make the comparison of the interatomic distances and DW factors as a function of temperature statistically significant. The validity of the analysis is proved as the best-fit interatomic distances resulted in excellent agreement with crystallographic data.[6–9] We are able to distinguish two Fe-O distances (octahedral and tetrahedral sites) in Fe_3O_4 (Table I). The local structure around the tetrahedral Fe_A atoms remains unaltered in the whole temperature range. However, a rather low value of the DW factor of the Fe_A-O distance is obtained compared to the one of the Fe_B-O distance. This can be understood in terms of the regular tetrahedral environment around the Fe_A atom, without a significant spread of Fe-O distances.[32] We note here that there is a strong correlation of the crystallographic distortion between Fe_B-O and Fe_A-O interatomic distances and the values of the respective DW factors. This introduces some restrictions in the fit and can explain the large statistical errors found for the DW factors of the Fe-O distance for the tetrahedral site.

In the following, we will discuss in detail the results obtained for the local structure around the octahedral Fe_B atom, where major changes are expected to occur at the Verwey transition. The temperature dependence of the average Fe_B

TABLE I. Best-fit structural parameters of the first oxygen coordination shell of $MnFe_2O_4$ and Fe_3O_4 at the Fe *K* edge. *N* is the coordination number (fixed), $R_{Fe(B)\text{-}O}$ and $R_{Fe(A)\text{-}O}$ are the average interatomic distances for the octahedral *B* and tetrahedral *A* site, respectively and σ^2 are the Debye-Waller factors. The overall reduction factor S_0^2 was fixed to 0.72 and numbers in parenthesis are statistical errors in the best significant digit.

$MnFe_2O_4$						
T (K)	*N*	$R_{Fe(B)\text{-}O}$ (Å)	$\sigma^2\times10^{-3}$ (Å^2)			
60	6	2.019(3)	5.4(4)			
85	6	2.012(2)	5.4(4)			
110	6	2.015(3)	5.4(4)			
130	6	2.015(3)	5.5(4)			
190	6	2.015(2)	5.8(4)			
250	6	2.015(2)	6.3(4)			
Fe_3O_4						
T (K)	*N*[a]	$R_{Fe(B)—O}$ (Å)	$\sigma^2\times10^{-3}$ (Å^2)	*N*[a]	$R_{Fe(A)—O}$ (Å)	$\sigma^2\times10^{-3}$ (Å^2)
60	4	2.062(5)	6.5(8)	1.34	1.891(5)	2.1(10)
85	4	2.062(5)	6.5(8)	1.34	1.890(5)	2.0(10)
100	4	2.062(5)	6.6(8)	1.34	1.890(5)	2.2(10)
110	4	2.065(5)	6.7(8)	1.34	1.893(5)	2.0(10)
120	4	2.065(5)	6.6(8)	1.34	1.893(5)	2.1(10)
130	4	2.063(5)	6.4(8)	1.34	1.891(5)	2.1(10)
150	4	2.063(5)	6.4(8)	1.34	1.891(5)	2.2(10)
190	4	2.064(5)	6.7(8)	1.34	1.892(5)	2.1(10)
230	4	2.064(5)	7.2(8)	1.34	1.893(5)	2.1(10)
250	4	2.066(5)	7.5(8)	1.34	1.894(5)	2.2(10)

[a]The coordination numbers in the EXAFS analysis of Fe_3O_4 are 4 instead of 6 for the octahedral *B* site and 1.34 instead of 4 for the tetrahedral *A* site since EXAFS averages over all the Fe atoms in magnetite and only two-thirds of the Fe atoms occupy octahedral sites, the remaining one-third occupies the tetrahedral ones.

-O interatomic distance and its DW factor for Fe_3O_4 and $MnFe_2O_4$ are compared in Fig. 3(a) and 3(b), respectively. A larger value of the average Fe_B-O distance is obtained for Fe_3O_4. This increase is correlated to the decrease in the formal valence state of the octahedral Fe ion for this compound, namely, $Fe^{+2.5}$ whereas it is Fe^{+3} for $MnFe_2O_4$. In both samples, the average Fe_B-O distance remains almost constant in the whole temperature range within the experimental error. Therefore, no discontinuity is observed across the Verwey transition in Fe_3O_4. The evolution of the DW factor of the Fe_B-O distance, $\sigma^2(T)$, shows a tiny discontinuity at T_V for Fe_3O_4 whereas $MnFe_2O_4$ displays the usual decrease as the temperature decreases due to the smaller thermal motion [Fig. 3(b)]. Figure 4 compares the relevant structural parameters of the second coordination shell around Fe_B in Fe_3O_4 and $MnFe_2O_4$ obtained by EXAFS. The interatomic [Fe_B-Fe_B and Fe_B-$Fe(Mn)_A$] distances remain almost constant in the whole temperature range for both compounds although a small discontinuity is observed at T_V for the Fe_B-Fe_B distance in the case of Fe_3O_4 [Fig. 4(a)]. Figure 4(b) shows the temperature dependence of σ^2 for both, Fe_B-Fe_B and Fe_B—$Fe(Mn)_A$ bonds in Fe_3O_4 and $MnFe_2O_4$. For $MnFe_2O_4$, DW factors of either the Fe_B-Fe_B or Fe_B-Mn_A distances display a standard thermal evolution, becoming lower as the temperature is lowered and the phonon vibration decreases. The same can be deduced for the σ^2 of the Fe_B-Fe_A distance in Fe_3O_4. On the other hand, a slight anomaly in the $\sigma^2(T)$ variation is observed at the phase transition for the Fe_B-Fe_B bonds in Fe_3O_4. Moreover, a rather larger σ^2 of these Fe_B-Fe_B distances is obtained for Fe_3O_4 than for $MnFe_2O_4$ in the whole temperature range, suggesting a larger spread of such distances in the former compound.

IV. DISCUSSION

Starting from the point that the Verwey MIT in magnetite is strongly correlated to the structural phase transition, the main task of this work was to explore the local structure around the octahedral Fe_B atom above and below T_V and how it changes in the MIT. Let us begin with the low-temperature insulating phase. The EXAFS data at $T=60$ K (Table I) give an average Fe_B-O distance of 2.062 ± 0.005 Å with an unusually high DW factor of about $6.5\pm0.8\times10^{-3}$ Å^2. This value agrees with the different crystallographic determinations[7–9] and it is bigger than the one obtained for $MnFe_2O_4$, 2.019 ± 0.003 Å with a DW factor of about

TABLE II. Best-fit structural parameters of the second coordination shell of $MnFe_2O_4$ and Fe_3O_4 at the Fe *K* edge. *N* is the coordination number (fixed); $R_{Fe(B)\text{-}Fe(B)}$, $R_{Fe(B)\text{-}Mn}$, $R_{Fe(B)\text{-}Fe(A)}$, and $R_{Fe(A)—Fe(A)}$ are the respective average interatomic distances and σ^2 are the Debye-Waller factors. The overall reduction factor S_0^2 was fixed to 0.72 and numbers in parenthesis are statistical errors in the best significant digit.

					$MnFe_2O_4$				
T (K)	*N*	$R_{Fe(B)\text{-}Fe(B)}$ (Å)	$\sigma^2\times10^{-3}$ (Å^2)	*N*	$R_{Fe(B)\text{-}Mn}$ (Å)	$\sigma^2\times10^{-3}$ (Å^2)			
60	6	3.012(2)	3.3(3)	6	3.534(4)	3.1(4)			
85	6	3.015(2)	3.5(2)	6	3.537(3)	3.5(4)			
110	6	3.012(2)	3.5(3)	6	3.535(4)	3.5(5)			
130	6	3.012(2)	3.7(3)	6	3.535(4)	3.8(5)			
190	6	3.012(3)	4.3(3)	6	3.536(5)	4.5(5)			
250	6	3.013(3)	4.9(3)	6	3.536(5)	5.4(6)			
					Fe_3O_4				
T (K)	N^a	$R_{Fe(B)\text{-}Fe(B)}$ (Å)	$\sigma^2\times10^{-3}$ (Å^2)	N^a	$R_{Fe(B)\text{-}Fe(A)}$ (Å)	$\sigma^2\times10^{-3}$ (Å^2)	N^a	$R_{Fe(A)\text{-}Fe(A)}$ (Å)	$\sigma^2\times10^{-3}$ (Å^2)
60	4	2.982(5)	8.2(7)	8	3.481(3)	4.4(4)	1.34	3.636(3)	4.4(4)
85	4	2.982(5)	8.2(7)	8	3.481(3)	4.4(3)	1.34	3.636(3)	4.4(3)
100	4	2.982(5)	8.2(7)	8	3.481(3)	4.6(3)	1.34	3.636(3)	4.6(3)
110	4	2.982(5)	8.2(7)	8	3.481(3)	4.7(4)	1.34	3.636(3)	4.7(4)
120	4	2.982(6)	8.2(7)	8	3.482(4)	4.9(4)	1.34	3.637(4)	4.9(4)
130	4	2.977(5)	7.8(7)	8	3.482(3)	4.8(4)	1.34	3.637(3)	4.8(4)
150	4	2.977(5)	7.8(7)	8	3.482(3)	5.2(4)	1.34	3.637(3)	5.2(4)
190	4	2.976(5)	8.0(7)	8	3.482(3)	5.6(4)	1.34	3.637(3)	5.6(4)
230	4	2.977(5)	8.3(7)	8	3.483(3)	6.2(5)	1.34	3.638(3)	6.2(5)
250	4	2.977(5)	8.7(7)	8	3.483(3)	6.5(5)	1.34	3.638(3)	6.5(5)

[a]The coordination numbers in the EXAFS analysis of Fe_3O_4 are calculated from the crystallographic ones on the basis that EXAFS averages over all the Fe atoms in magnetite and only two-thirds of the Fe atoms occupy octahedral sites and the remaining one-third occupies the tetrahedral ones.

$5.4\pm0.4\times10^{-3}$ Å^2, according to the distinct formal valence state. The fact that few Mn atoms could replace Fe ones at the octahedral site in $MnFe_2O_4$ would induce an apparent increase of the DW factor. This could explain the high value resulted for the DW factor of the Fe_B-O distance in $MnFe_2O_4$ despite a regular octahedral environment is present. Furthermore, the σ^2 of the Fe_B-O distance is even higher for Fe_3O_4. This result can be understood due to the expected higher distortion of the FeO_6 octahedra in Fe_3O_4. We note here that $MnFe_2O_4$ only has formal Fe_B^{3+} in a cubic structure with a unique Fe_B-O distance, whereas Fe_3O_4 has Fe_B atoms in a mixed valence state distributed over at least 16 nonequivalent FeO_6 local environments.[6,8] The absolute value of σ^2 in Fe_3O_4 agrees well with the static distortion below T_V determined by several crystallographic studies.[7–9] Figure 5 shows the fit of the first-shell EXAFS signal of Fe_3O_4 at $T=60$ K, considering a unique Fe_B-O and a unique Fe_A—O, distances for the octahedral and tetrahedral sites, respectively. The excellent agreement with the experimental data prevents us the use of further contributions. However, we attempted to simulate the experimental signal using two kinds of octahedra (namely, $Fe^{2+}O_6$ and $Fe^{3+}O_6$ with average Fe-O distances of 2.160 and 2.025 Å, respectively,[33] resulting in a remarkably worse agreement. Therefore, the previous results support the presence of a pure mixed-valent octahedral Fe in Fe_3O_4, even below T_V.[18,19]

Upon heating, the first-order structural transition from the distorted monoclinic phase at low temperatures to the room-temperature cubic phase occurs at T_V where the resistivity abruptly decreases by two orders of magnitude. Our EXAFS analysis shows no significant variation in the local structure for the FeO_6 octahedra above and below T_V (see Fig. 3), contrary to the expected behavior for the melting of the CO state. This means that the local distortions are already present in the pseudocubic phase above T_V and change from dynamic to static at the Verwey MIT. To check this result, we have subtracted the EXAFS spectra at the different temperatures up to 250 K from the spectrum at $T=60$ K. The FT of the *k*-weighted difference spectra were calculated between 3.5 and 16 Å^{-1} using a Gaussian window and they are displayed in Fig. 6. There is no peak (out of the noise level) between 1 and 2 Å, which corresponds with the first coordination shell of 6 O atoms, confirming that the average FeO_6 local environment remains unaltered through the transition. Moreover, XANES spectra across T_V are alike. The maximum difference between the spectra at various temperatures crossing the transition is less than 0.2% of the total absorption (see Fig. 7). Accordingly, the local electronic and geometric structure

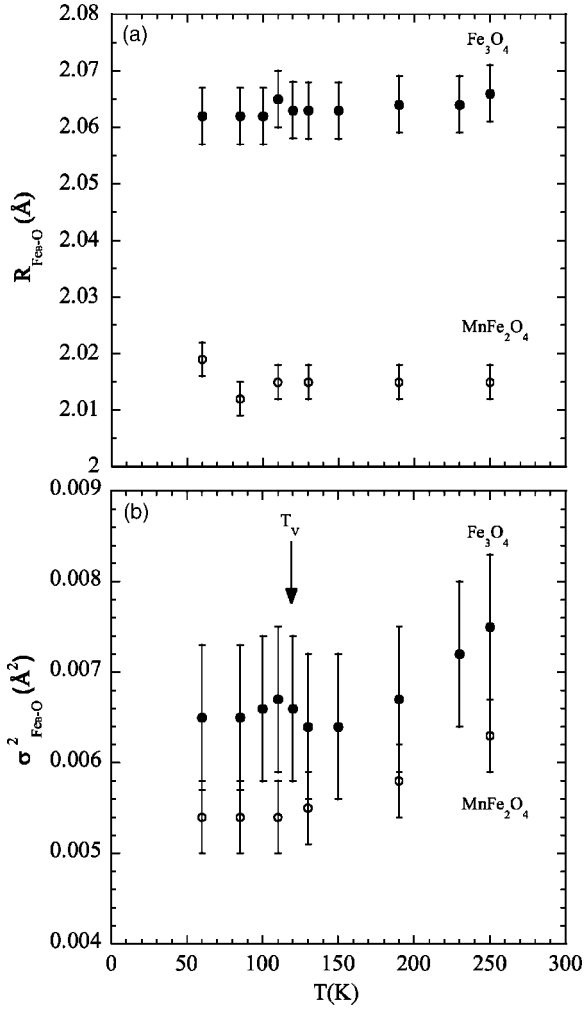

FIG. 3. Temperature dependence of (a) interatomic Fe-O distance and (b) Debye-Waller factor of the Fe-O bond distribution around the octahedral Fe_B atoms determined by EXAFS. Closed and open circles indicate data for Fe_3O_4 and $MnFe_2O_4$, respectively.

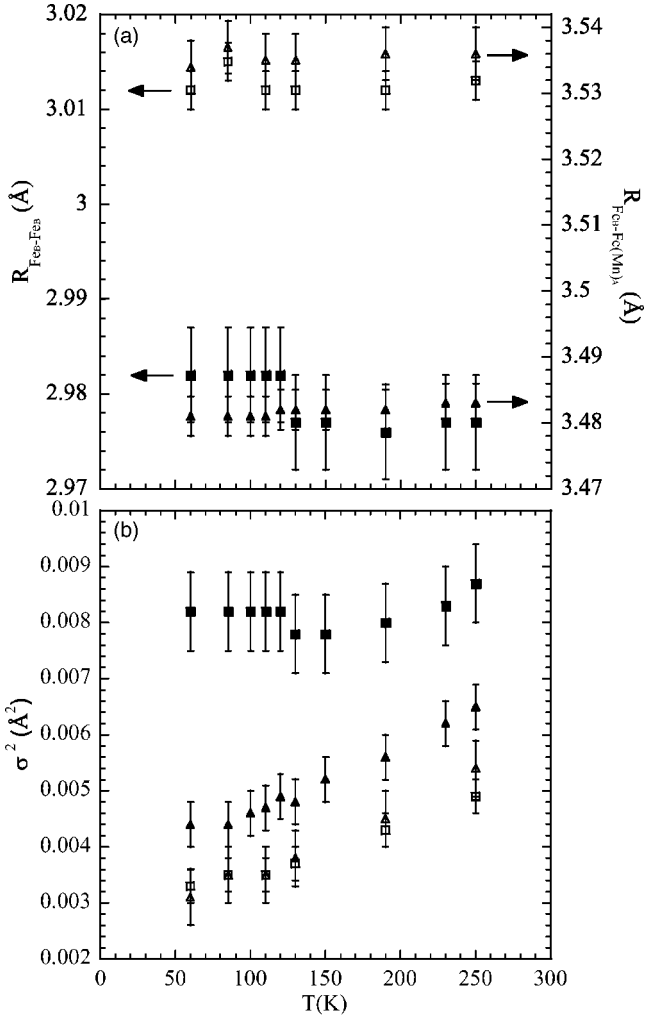

FIG. 4. Temperature dependence of (a) interatomic Fe_B-Fe_B (squares) and Fe_B-$Fe(Mn)_A$ (up-triangles) distances and (b) Debye-Waller factors of the second coordination shell around the octahedral Fe_B atoms determined by EXAFS. Closed and open symbols indicate data for Fe_3O_4 and $MnFe_2O_4$ samples, respectively.

around the octahedral Fe atom barely changes across the Verwey MIT in Fe_3O_4, in line with previous x-ray scattering experiments.[18] However, differences are clearly detectable in the Fourier transform of the difference spectra between 2.5 and 3.5 Å. We observe changes in both, the first peak (centered near 2.97 Å) corresponding to the shell of 6 Fe_B atoms and the second peak (centered near 3.5 Å) predominantly arising from both, the 6 Fe_A atoms around the B sites and the 12 Fe_B atoms around the A sites. We observe that the intensity of the two peaks increases with increasing temperature, as expected from the standard behavior of thermal vibrations. It is noteworthy that there is a discontinuity in the temperature range of 120–130 K, crossing T_V, giving direct signature of the phase transition. This result suggests that the Verwey MIT in magnetite must be correlated with instability in the local structure beyond the first oxygen coordination shell, i.e. associated with the Fe-Fe second coordination shell. The structural analysis of the second coordination shell reveals an anomalously high Debye-Waller factor for the Fe_B-Fe_B octahedral distance in Fe_3O_4 compared to $MnFe_2O_4$ in the whole temperature range [Fig. 4(b) and Table II]. This means that the instability mainly concerns the octahedral Fe chains and phonon modes with displacements along these chains will play an important role in the dynamics of this system.

Based on the former discussion, we propose a new picture for the Verwey MIT. Fe_3O_4 has a local distortion of the Fe_BO_6 octahedra that it is dynamic above T_V. In other words, the high-temperature structure is similar to the low temperature one but the lack of coherence in the dynamic local distortions among the different unit cells, makes the average lattice show a higher symmetry, namely, the cubic Fd-3m. Below T_V, a long-range order of the local distortions is established giving rise to the monoclinic structure. The existence of this short-range structural ordering above T_V is supported by neutron and x-ray diffuse scattering experiments[21,22] although we have shown that it does not imply electronic CO. On the other hand, if the low-temperature local structure remains near unaltered crossing T_V, we will expect to find at least more than one octahedral and one tetrahedral Fe atoms in the cubic phase. However, NMR[34,16] and Mössbauer[35] experiments only observe two

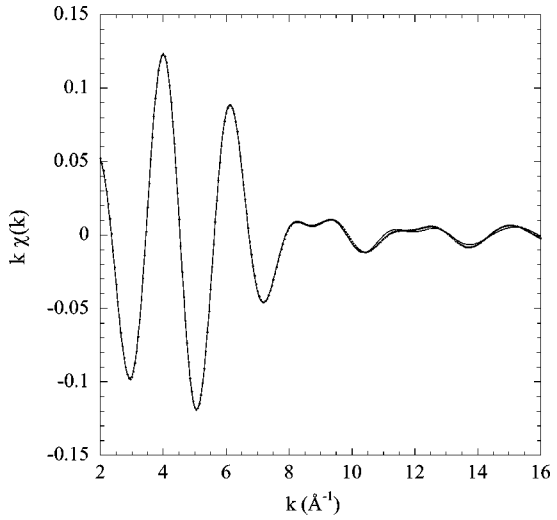

FIG. 5. First-shell Fourier filtered EXAFS signal (dotted line) of Fe_3O_4 at the Fe *K* edge at $T=60$ K (below T_V) compared to best-fit (solid line) obtained using only two Fe-O shells, one for the octahedral and the other one for the tetrahedral Fe sites.

different Fe atoms above T_V (octahedral and tetrahedral), apparently contradicting this result. It is noteworthy that the characteristic time for these experiments is $\sim 10^{-8}$ s, longer than for XAFS measurements ($\sim 10^{-15}$ s) so they cannot discriminate fluctuations of the order of thermal vibrations.

After discarding the order-disorder-type electronic CO model, it is still intriguing the conduction mechanism of Fe_3O_4. Magnetite is an electrical insulator below T_V, as the rest of spinel ferrites. Why does it become conductor above T_V? According to our model, the Verwey transition is an order-disorder-type structural phase transition where local distortions are dynamically disordered in the metallic phase (high-temperature). The insulating phase (low-temperature)

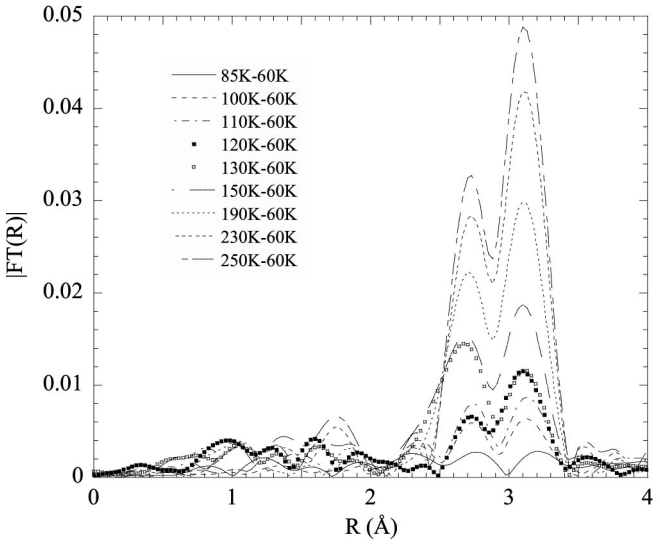

FIG. 6. Fourier transform modulus of the difference obtained by subtracting the *k*-weighted EXAFS spectra of Fe_3O_4 at the Fe *K* edge taken at fixed temperatures from 85 K up to 250 K from the spectrum at $T=60$ K.

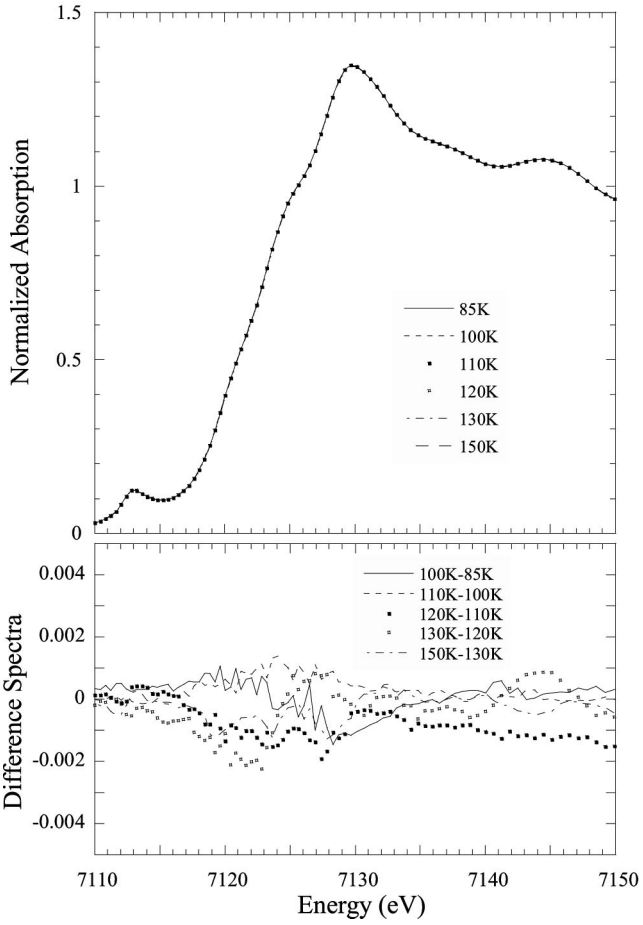

FIG. 7. Upper panel: Normalized XANES spectra of Fe_3O_4 at the Fe *K* edge at temperatures close to T_V. Lower panel: A comparison of the differences between the XANES spectra at successive temperatures across this MIT transition.

results from the ordering of these local distortions by the condensation of particular phonon modes. Then, the lattice dynamics is responsible for the transport properties. In other words, charge carriers are coupled to the phonon modes associated with the stabilization of the local distortions in such a way that the vibrational atomic motion determines the mobility of these carriers. The opening of a gap at T_V due to the softening of these phonon modes should then cause the insulating state below T_V. This conduction mechanism has already been proposed to explain the electrical behavior of $LaMnO_3$ across the so-called orbital ordering (Jahn-Teller) transition at $T_{JT} \sim 750$ K.[36] $LaMnO_3$ is an insulator below T_{JT} and an abrupt drop in the electrical resistivity occurs at T_{JT}, the system becoming metallic.[37] As in magnetite but even much more evident, the Jahn-Teller Mn^{3+} ion is already dynamically distorted above T_{JT} fluctuating among the three equivalent tetragonal configurations of the MnO_6 octahedron. Below T_{JT}, these tetragonal distortions are periodically ordered (static phase). The electronic orbital of the e_g electron couples to the three possible distortions giving rise to three degenerate vibronic states. The electron thermally excited jumps between these states at $T > T_{JT}$ and is localized in an ordered state below T_{JT} due to the ordering of the local tetragonal distortions. Similar results were also obtained for

the so-called CO manganites.[38] These samples show a dynamical distorted octahedron around the Mn atoms in the paramagnetic (high-temperature) phase. Upon decreasing temperature, the distortion is frozen giving rise to the so-called charge-ordered phase. A discontinuity of the electrical conductivity is observed at this phase transition that can be explained as arising from the change of the lattice dynamics.

Obviously, the proposed conduction mechanism is phonon-mediated but it cannot be considered as polaronic either in terms of a narrow polaron-band model[3,5] or in terms of "large polarons" as in Yamada's molecular polaron model.[27] It is more suitable to speak in terms of collective electron-phonon coupled states (vibronic states) in the sense that the electrical conduction should be mediated by formally "large polarons," extending beyond an interatomic Fe-O distance. The importance of the electron-lattice interactions on the Verwey transition mechanism has already been noted by studying the heat capacity, neutron scattering and elastic constants on slightly doped and nonstoichiometric magnetite (Ref. 39 and references contained therein). It was found that the character of the Verwey MIT changes from first to second or higher order with doping or oxygen nonstoichiometry, disappearing beyond a critical composition. This result indicates that a minimum correlation length is needed for the occurrence of the MIT and confirms that electronic localization cannot occur at the atomic level as it has been previously stated. A recent work[28] has also tried to overcome the localization on the atom, i.e., the CO picture, based on a strong electron-phonon interaction. In fact, Seo *et al.* argue that the Verwey transition can be considered as a transition from a ferro-orbital ordered metallic phase at $T > T_V$ toward an insulating phase due to the formation of bond dimerization of two Fe_B ions through a Peierls lattice distortion below T_V. This model provides a nice mechanism for the appearing of an insulating state in magnetite. However, it cannot be considered as a general solution because there are no experimental evidences of a lower symmetry than the cubic one for the high-temperature phase, which directly contradicts the prediction of a ferro-orbital ordered metallic phase at $T > T_V$.

V. CONCLUSION

In summary, we conclude that the local structure around either the octahedral or tetrahedral Fe atoms in magnetite remains nearly unaltered crossing the Verwey transition. The phase transition is caused by a change in the regime of the local distortions from a static regime at low temperatures to a dynamical one at high temperatures, i.e., an order-disorder structural type. Phonon modes associated with displacements of the octahedral Fe-Fe chains are responsible for the lattice distortion. We propose that the dynamics of the local distortions above T_V are the origin of the electrical conductivity. Finally, this kind of vibronic conductivity mechanism provides a new framework to understand the electronic conduction in other transition-metal oxides.

ACKNOWLEDGMENTS

This work was financially supported by the Spanish CICyT MAT02-01221 project and DGA. We also acknowledge the ESRF and BM29 beam line for granting beam time.

*Corresponding author. Email address: jgr@unizar.es

[1] N. Tsuda, K. Nasu, A. Yanase, and K. Siratori, *Electronic Conduction in Oxides* (Springer, Berlin, 1990).

[2] M. Imada, A. Fujimori, and Y. Tokura, Rev. Mod. Phys. **70**, 1039 (1998).

[3] N.F. Mott, in *Proceedings of the International Meeting on Magnetite and Other Materials Showing a Verwey Transition, Cambridge, 1979* [(Philos. Mag. B **42** (3) (1980), special issue].

[4] J. M. Honig, in *The Metallic and Non-Metallic States of Matter*, edited by P. P. Edwards and C. N. Rao (Taylor and Francis, London, 1985, p. 261).

[5] N. F. Mott, *Metal-Insulator Transitions*, 2nd ed. (Taylor and Francis, London, 1990).

[6] V. A. M. Brabers, *Progress in Spinel Ferrite Research in Handbook of Magnetic Materials*, edited by K. H. J. Buschow (Elsevier Science B. V., Amsterdam, 1995), Vol. 8, p. 189.

[7] M. Iizumi, T. F. Koetzle, G. Shirane, S. Chikazumi, M. Matsui, and S. Todo, Acta Crystallogr., Sect. B: Struct. Crystallogr. Cryst. Chem. **38**, 2121 (1982).

[8] J. M. Zuo, J. C. H. Spence, and W. Petuskey, Phys. Rev. B **42**, 8451 (1990).

[9] J. P. Wright, J. P. Attfield, and P. G. Radaelli, Phys. Rev. Lett. **87**, 266401 (2001); J. P. Wright, J. P. Attfield, and P. G. Radaelli, Phys. Rev. B **66**, 214422 (2002).

[10] E. J. W. Verwey, Nature (London) **144**, 327 (1939); E. J. W. Verwey and P. W. Haayman, Physica (Amsterdam) **8**, 979 (1941).

[11] J. R. Cullen and E. R. Callen, Phys. Rev. B **7**, 397 (1973).

[12] Z. Zhang and S. Satpathy, Phys. Rev. B **44**, 13 319 (1991); V. I. Anisimov, I. S. Elfimov, N. Hamada, and K. Terakura, Phys. Rev. B **54**, 4387 (1996); A. Yanase and N. Hamada, J. Phys. Soc. Jpn. **68**(5), 1607 (1999).

[13] Z. Szotek, W. M. Temmerman, A. Svane, L. Petit, G. M. Stocks, and H. Winter, Phys. Rev. B **68**, 054415 (2003); I. Leonov, A. N. Yaresko, V. N. Antonov, M. A. Korotin, and V. I. Anisimov, Phys. Rev. Lett. **93**, 146404 (2004); H. T. Jeng, G. Y. Guo, and D. J. Huang, Phys. Rev. Lett. **93**, 156403 (2004).

[14] M. Mizoguchi, J. Phys. Soc. Jpn. **44**, 1501 (1978); J. Phys. Soc. Jpn. **44**, 1512 (1978).

[15] J. García and G. Subías, J. Phys.: Condens. Matter **16**, R145 (2004).

[16] P. Novak, H. Stepankova, J. Englich, J. Kohout, and V. A. M. Brabers, Phys. Rev. B **61**, 1256 (2000).

[17] M. Mizoguchi, J. Phys. Soc. Jpn. **70**, 2333 (2001).

[18] J. García, G. Subías, M. G. Proeitti, H. Renevier, Y. Joly, J. L. Hodeau, J. Blasco, M. C. Sánchez, and J. F. Bérar, Phys. Rev. Lett. **85**, 578 (2000); J. García, G. Subías, M. G. Proeitti, J. Blasco, H. Renevier, J. L. Hodeau, and Y. Joly, Phys. Rev. B **63**, 054110 (2001).

[19] G. Subias, J. García, J. Blasco, M. G. Proietti, H. Renevier, and

M. C. Sánchez, Phys. Rev. Lett. **93**, 156408 (2004).
[20] S. Todo, N. Takeshita, T. Kanehara, T. Mori, and N. Mori, J. Appl. Phys. **89**(11), 7347 (2001).
[21] Y. Fujii, G. Shirane, and Y. Yamada, Phys. Rev. B **11**, 2036 (1975); S. M. Shapiro, M. Iizumi, and G. Shirane, Phys. Rev. B **14**, 200 (1976).
[22] T. Toyoda, S. Sasaki, and M. Tanaka, Jpn. J. Appl. Phys., Part 1 **36**, 2247 (1997).
[23] M. Matsui, S. Todo, and S. Chikazumi, J. Phys. Soc. Jpn. **42**(5), 1517 (1977); S. Takai, Y. Akishige, H. Kawaji, T. Atake, and E. Sawaguchi, J. Chem. Thermodyn. **26**, 1259 (1994).
[24] A. Chainani, T. Tokoya, T. Moritomo, T. Takahashi, and S. Todo, Phys. Rev. B **51**, 17976 (1995).
[25] J. H. Park, L. H. Tjeng, J. W. Allen, P. Metcalf, and C. T. Chen, Phys. Rev. B **55**, 12813 (1997).
[26] S. K. Park, T. Ishikawa, and Y. Tokura, Phys. Rev. B **58**, 3717 (1998).
[27] Y. Yamada, N. Wakabayashi, and R. M. Nicklow, Phys. Rev. B **21**, 4642 (1980).
[28] H. Seo, M. Ogata, and H. Fukuyama, Phys. Rev. B **65**, 085107 (2002).
[29] A. Filipponi, M. Borowski, D.T. Bowron, S. Ansell, A. Di Cicco, S. de Panfilis, and J.P. Itiè, Rev. Sci. Instrum. **71**, 2422 (2000).
[30] D. C. Koningsberger and R. Prins, *X-ray Absorption: Principles, Application, Techniques of EXAFS, SEXAFS and XANES* (Wiley, New York, 1988).
[31] J. J. Rehr and R. C. Albers, Rev. Mod. Phys. **72**, 621 (2000); see http://FEFF.phys.washington.edu/
[32] Note: EXAFS analysis of the first oxygen coordination shell of $ZnFe_2O_4$ at the Zn *K*-edge gives a similar value of $\sigma^2_{Zn—O} = 0.0024 \pm 0.0004$ Å^2 at room temperature. It is noteworthy that $ZnFe_2O_4$ is a normal spinel, as $MnFe_2O_4$, and Zn atoms occupy the tetrahedral sites.
[33] R. D. Shannon, Acta Crystallogr., Sect. A: Cryst. Phys., Diffr., Theor. Gen. Crystallogr. **32**, 751 (1976).
[34] N. N. Kovtum and A. A. Shamiakov, Solid State Commun. **13**, 1345 (1973); K. Yanai, M. Mizoguchi, and S. Iida, J. Phys. Soc. Jpn. **50**, 65 (1981).
[35] W. Künding and R. R. Hardrove, Solid State Commun. **7**, 223 (1969).
[36] M. C. Sánchez, G. Subías, J. García, and J. Blasco, Phys. Rev. Lett. **90**, 045503 (2003).
[37] J.-S. Zhou and J. B. Goodenough, Phys. Rev. B **60**, R15002 (1999).
[38] G. Subías, J. García, J. Blasco, M. C. Sánchez, and M. G. Proietti, J. Phys.: Condens. Matter **14**, 5017 (2002).
[39] Z. Kakol and A. Koslowski, Solid State Sci. **2**, 737 (2000).